

A strongly conservative finite element method for the coupling of Stokes and Darcy flow

G. Kanschat^{a,*}, B. Rivière^{b,2}

^a Department of Mathematics, Texas A&M University, 3368 TAMU, College Station, TX 77843-3368, United States

^b Department of Computational and Applied Mathematics, Rice University, 6100 Main Street, MS-134, Houston, TX 77005-1892, United States

ARTICLE INFO

Article history:

Received 12 August 2009

Received in revised form 6 April 2010

Accepted 13 April 2010

Available online 27 April 2010

Keywords:

Stokes flow

Darcy flow

Beavers–Joseph–Saffman condition

Finite element method

Mixed finite elements

Discontinuous Galerkin

Multiphysics

ABSTRACT

We consider a model of coupled free and porous media flow governed by Stokes and Darcy equations with the Beavers–Joseph–Saffman interface condition. This model is discretized using divergence-conforming finite elements for the velocities in the whole domain. Discontinuous Galerkin techniques and mixed methods are used in the Stokes and Darcy sub-domains, respectively. This discretization is strongly conservative in $H^{\text{div}}(\Omega)$ and we show convergence. Numerical results validate our findings and indicate optimal convergence orders.

© 2010 Elsevier Inc. All rights reserved.

1. Introduction

The coupling of Stokes and Darcy equations arises from the modeling of groundwater contamination through streams and filtration problems [25,19]. In this work, a new numerical method is proposed, that employs divergence-conforming velocity spaces, i.e. spaces included in $H^{\text{div}}(\Omega)$. The Darcy flow is discretized by a mixed finite element method and the Stokes flow by a mixed (velocity–pressure) discontinuous Galerkin (DG) method. The two types of flow are coupled by appropriate interface conditions, namely mass conservation, balance of forces across the interface and the Beavers–Joseph–Saffman law [6,30,20–22].

One advantage of our approach is that mass conservation in the sense of $H^{\text{div}}(\Omega)$ is achieved. In particular, if there are no sources or sinks, the divergence of the velocity is an $L^2(\Omega)$ function and it is zero in that space (see [12]). This implies that the divergence of the velocity is pointwise equal to zero inside the mesh cells. Therefore, we refer to this method as *strongly conservative*. It differs from a weakly conservative method, where mass conservation is only guaranteed when testing with functions in the discrete pressure space; the result is usually a scheme which is locally (cellwise) conservative, but not pointwise.

Another advantage is that the bilinear form only involves one term on the interface. Indeed only the tangential component of the velocity from the Beavers–Joseph–Saffman law appears in the scheme. Finally this paper proposes and analyzes a

* Corresponding author.

E-mail address: kanschat@tamu.edu (G. Kanschat).

¹ Supported in part by the National Science Foundation through Grant Nos. DMS-0713829 and DMS-0810387 and by the King Abdullah University of Science and Technology (KAUST) through Award No. KUS-C1-016-04.

² Supported in part by the National Science Foundation through Grant No. DMS-0810422.

general framework as the scheme is valid for various DG methods, such as the local discontinuous Galerkin and the interior penalty methods.

Various numerical methods, such as finite element methods, mixed methods, discontinuous Galerkin methods and combinations of these methods, have been studied in the literature. For instance, finite element methods were studied in [14] and finite element methods coupled with mixed methods have been analyzed in [24]. Primal DG methods using broken Sobolev spaces are analyzed in [27], and they are coupled with mixed methods in [29]. All of these methods exhibit some mass loss depending on the accuracy of the discretization, which is the main reason to propose our new scheme. A conforming mixed method is analyzed in [15]. Stabilized methods are considered in [10,11,1].

The plan of the paper is as follows. Section 2 defines the model problem and a corresponding weak formulation. The general scheme is described in Section 3. Its analysis is presented in Section 4. Finally, Section 5 shows numerical examples and conclusions follow.

2. Model problem and weak formulation

Let Ω be a bounded polygonal domain in \mathbb{R}^d , $d = 2, 3$. We assume that Ω is divided into two regions Ω_S and Ω_D , each being a union of polygonal subdomains. Denote by Γ_{SD} the polygonal line that is the interface between Ω_S and Ω_D . The external boundaries are defined by

$$\Gamma_S = \partial\Omega \cap \partial\Omega_S, \quad \Gamma_D = \partial\Omega \cap \partial\Omega_D.$$

In the region Ω_S the fluid velocity u_S and fluid pressure p_S satisfy the Stokes equations:

$$-\nabla \cdot (2\nu D(u_S)) + \nabla p_S = f_S, \quad \text{in } \Omega_S, \quad (1a)$$

$$\nabla u_S = 0, \quad \text{in } \Omega_S, \quad (1b)$$

$$u_S = 0, \quad \text{on } \Gamma_S. \quad (1c)$$

The deformation tensor is $D(u_S) = \frac{1}{2}(\nabla u_S + (\nabla u_S)^T)$. The coefficient $\nu > 0$ is the dimensionless fluid viscosity and the function f_S is a body force.

In the region Ω_D the fluid velocity u_D and fluid pressure p_D satisfy the Darcy equations:

$$\nabla \cdot u_D = f_D, \quad \text{in } \Omega_D, \quad (2a)$$

$$u_D + K\nabla p_D = 0, \quad \text{in } \Omega_D, \quad (2b)$$

$$u_D \cdot n = 0, \quad \text{on } \Gamma_D. \quad (2c)$$

Here, f_D models sinks and sources in the porous medium. The coefficient $K > 0$ is the dimensionless permeability of the porous medium.

The system of equations is completed by the Beavers–Joseph–Saffman transmissibility conditions at the interface. Let n and τ denote unit normal and tangential vectors to Γ_{SD} , respectively. We assume that n points outward of Ω_S . Introducing the phenomenological friction coefficient $\gamma > 0$, these conditions read:

$$u_S \cdot n = u_D \cdot n, \quad (3a)$$

$$p_S - 2\nu D(u_S)n \cdot n = p_D, \quad (3b)$$

$$\gamma K^{-1/2} u_S \cdot \tau - 2\nu D(u_S)n \cdot \tau = 0. \quad (3c)$$

We remark that for three-dimensional domains, Eq. (3b) is satisfied for all tangential vectors to the interface. In order to obtain weak solutions to the set of Eqs. (1c), (2a)–(2c), (3a)–(3c) we introduce the spaces

$$H^{\text{div}}(\Omega) = \left\{ v \in L^2(\Omega) \mid \nabla \cdot v \in L^2(\Omega) \right\},$$

$$H_0^{\text{div}}(\Omega) = \left\{ v \in H^{\text{div}}(\Omega) \mid v \cdot n = 0 \text{ on } \partial\Omega \right\}.$$

In the subdomain Ω_S , we have to require additionally, that functions are weakly differentiable. Furthermore, if we use the space $H_0^{\text{div}}(\Omega)$, pressure functions will be determined only up to a constant. Thus, the function spaces for our weak formulation will be

$$Q = \left\{ q \in L^2(\Omega) \mid \int_{\Omega} q \, dx = 0 \right\},$$

$$V = \left\{ v \in H_0^{\text{div}}(\Omega) \mid v|_{\Omega_S} \in H^1(\Omega_S) \right\}.$$

We also use the standard notation $H^s(\mathcal{O})$ for the Sobolev space of order s on a bounded domain \mathcal{O} . We use the scalar product notation and norm on Ω , boundaries, faces, and subsets of those, namely

$$\begin{aligned}
 (\phi, \psi)_\Omega &= \int_\Omega \phi \odot \psi \, dx, & \langle \phi, \psi \rangle_\Gamma &= \int_\Gamma \phi \odot \psi \, ds, \\
 \|\phi\|_\Omega &= \left(\int_\Omega |\phi|^2 \, dx \right)^{1/2}, & \|\phi\|_\Gamma &= \left(\int_\Gamma |\phi|^2 \, ds \right)^{1/2}.
 \end{aligned}$$

The pointwise multiplication operator $\phi \odot \psi$ refers to the product $\phi\psi$, the scalar product $\phi \cdot \psi$ and the double contraction $\phi:\psi$ for scalar, vector and tensor arguments, respectively. The modulus $|\phi| = \sqrt{\phi \odot \phi}$ is defined accordingly.

On V and Q , we introduce the bilinear forms

$$\begin{aligned}
 a_D(u, v) &= (K^{-1}u, v)_{\Omega_D}, & \forall u, v \in V, \\
 a_S(u, v) &= 2\nu(D(u), D(v))_{\Omega_S}, & \forall u, v \in V, \\
 a_I(u, v) &= \gamma K^{-1/2} \langle u_S \cdot \tau, v_S \cdot \tau \rangle_{\Gamma_{SD}}, & \forall u, v \in V, \\
 a(u, v) &= a_D(u, v) + a_I(u, v) + a_S(u, v), & \forall u, v \in V, \\
 b(v, q) &= -(\nabla \cdot v, q)_\Omega, & \forall v \in V, \forall q \in Q.
 \end{aligned} \tag{4}$$

Throughout the paper, we use the notation $v_S = v|_{\Omega_S}$. Thus, $u_S \cdot \tau$ and $v_S \cdot \tau$ refer to the tangential traces of u and v taken from the side of Ω_S at the interface Γ_{SD} . The weak formulation of the problem (1c), (2a)–(2c), (3a)–(3c) reads: find $(u, p) \in V \times Q$ such that

$$\begin{aligned}
 a(u, v) + b(v, p) &= (f_S, v)_{\Omega_S}, & \forall v \in V, \\
 b(u, q) &= (f_D, q)_{\Omega_D}, & \forall q \in Q.
 \end{aligned} \tag{5}$$

3. Discretization

Let \mathbb{T}_h be a conforming triangulation of Ω such that the interface Γ_{SD} is the union of element edges. For any element $T \in \mathbb{T}_h$, we denote by h_T its diameter and we denote by h the maximum diameter over all mesh elements. Denote by I_h^S the set of edges that are interior to Ω_S . Denote by \mathbb{T}_h^S the set of mesh elements that belong to Ω_S .

As above, we use the scalar product and norm notation on \mathbb{T}_h , boundaries, faces, and subsets of those, namely

$$\begin{aligned}
 (u, v)_{\mathbb{T}_h} &= \sum_{T \in \mathbb{T}_h} \int_T u \cdot v \, dx, & \langle u, v \rangle_{\Gamma_h^S} &= \sum_{F \in \Gamma_h^S} \int_F u \cdot v \, ds, \\
 \|u\|_{\mathbb{T}_h} &= \left(\sum_{T \in \mathbb{T}_h} \int_T u^2 \, dx \right)^{1/2}, & \|u\|_{\Gamma_h^S} &= \left(\sum_{F \in \Gamma_h^S} \int_F u^2 \, ds \right)^{1/2}.
 \end{aligned}$$

For the discrete spaces, we use pairs of a divergence-conforming velocity space $V_h \subset H_0^{\text{div}}(\Omega)$ and the matching pressure space $Q_h \subset Q$, that is of order k (see Table 1 for examples of admissible pairs of finite element spaces). The Stokes operator is discretized by a DG method. In order to do so, we introduce further notation. The jump of traces of a discontinuous function v across interior faces of the mesh is denoted by $[[v]]$. The following DG norm is used:

$$\|v\|_{1,h} = \left(\|\nabla v\|_{\mathbb{T}_h^S}^2 + \frac{\sigma}{h} \|[[v]]\|_{\Gamma_h^S}^2 + \frac{2\sigma}{h} \|v\|_{\Gamma_h^S}^2 \right)^{1/2}, \tag{6}$$

where the parameter $\sigma \geq 0$ is the usual penalty parameter of order k^2 . Note that the notation above applies only to quasi-uniform meshes of isotropic cells. On non-uniform meshes, this quantity has to be localized, and on anisotropic cells, the cell size orthogonal to the face should be used and the quotient averaged from both sides, see e.g. [18,23]. For Navier–Stokes equations, the BDM pair was suggested in [12], the Raviart–Thomas pair in [13] (see also [31]).

3.1. Abstract assumptions

In what follows, we present an analysis that is valid for various DG methods and finite element spaces. Therefore, we will list conditions on the discretization scheme as a list of assumptions and discuss examples in the following subsection.

Table 1
Velocity spaces and matching pressure spaces.

	Triangles/tetrahedra	Quadrilaterals/hexahedra
V_h	Q_h	Q_h
BDM $_{k+1}$	\mathbb{P}_k	\mathbb{P}_k
\mathbb{RT}_k	\mathbb{P}_k	\mathbb{Q}_k
BDFM $_{k+1}$	\mathbb{P}_k	\mathbb{P}_k
ABF $_k$		\mathbb{Q}_k

Assumption 1.

$$\nabla \cdot V_h \subset Q_h. \quad (7)$$

Our analysis is based on the existence of a projection operator Π_h that satisfies several properties.

Assumption 2. There exists a projection operator $\Pi_h : H_0^{\text{div}}(\Omega) \rightarrow V_h$, satisfying the following properties:

1. Let $P_h : Q \rightarrow Q_h$ be the L^2 -projection. The commutation property

$$(q, \nabla \cdot \Pi_h v)_\Omega = (P_h q, \nabla \cdot v)_\Omega \quad (8)$$

holds for all $v \in V$ and $q \in Q$.

2. The value of $\Pi_h v$ on a grid cell K depends on the values of v on K and ∂K only.

3. Π_h is stable in $L^2(\Omega)$, $H^{\text{div}}(\Omega)$ and $L^2(\Gamma_{SD})$: there exists a constant C_s independent of h_K and h , such that

$$\|\Pi_h v\|_K \leq C_s \|v\|_K, \quad (9a)$$

$$\|\nabla \cdot \Pi_h v\|_K \leq C_s \|\nabla \cdot v\|_K, \quad (9b)$$

$$\|(\Pi_h w)_S\|_{\Gamma_{SD}} \leq C_s \|w_S\|_{\Gamma_{SD}}, \quad (9c)$$

for any $v \in H^{\text{div}}(K)$ and for any $w \in (H^1(\Omega_S))^d$.

4. Π_h is stable in the DG norm: there exists a constant C_s independent of h such that

$$\|\Pi_h v\|_{1,h} \leq C_s \|v\|_{1,h}. \quad (10)$$

5. For any $u \in H^{s+1}(\Omega)$ and $s \geq 1$, there is a constant C_a independent of h such that

$$\|u - \Pi_h u\|_{\Omega_D} \leq C_a h^{\min(k,s)+1} \|u\|_{H^{s+1}(\Omega_D)}, \quad (11a)$$

$$\|(u_S - (\Pi_h u)_S) \cdot \tau\|_{\Gamma_{SD}} \leq C_a h^{\min(k,s)+1/2} \|u\|_{H^{s+1}(\Omega_S)}, \quad (11b)$$

$$\|u - \Pi_h u\|_{1,h} \leq C_a h^{\min(k,s)} \|u\|_{H^{s+1}(\Omega_S)}. \quad (11c)$$

Now, consider the vector-valued elliptic problem

$$\begin{aligned} -2\nu \nabla \cdot D(\tilde{u}) &= f, \quad \text{in } \Omega_S, \\ \tilde{u} &= 0, \quad \text{on } \Gamma_S, \\ 2\nu D(\tilde{u})n &= 0, \quad \text{on } \Gamma_{SD}, \end{aligned} \quad (12)$$

which corresponds to the Stokes problem (1c) without the incompressibility constraint. Without restricting to a particular method, we abstractly introduce its DG discretization

$$a_{S,h}(\tilde{u}_h, v) = (f, v), \quad \forall v \in V_h. \quad (13)$$

The bilinear form $a_{S,h}(\cdot, \cdot)$ may correspond to any DG method fulfilling the following assumption.

Assumption 3. With \tilde{u} the solution to the vector-valued Eq. (12) we make the following assumptions on the discretizing DG bilinear form $a_{S,h}(\cdot, \cdot)$:

- **Boundedness:** there is a constant c_a independent of ν and the mesh size h such that for any u and v in V_h

$$|a_{S,h}(u, v)| \leq \nu c_a \|u\|_{1,h} \|v\|_{1,h}. \quad (14a)$$

- **Stability:** there is a positive constant α independent of ν and the mesh size h such that for any $u \in V_h$

$$a_{S,h}(u, u) \geq \nu \alpha \|u\|_{1,h}^2. \quad (14b)$$

- **Consistency:** for the solution \tilde{u} above and any $v \in V_h$ there holds

$$a_{S,h}(\tilde{u}, v) = (f, v)_{\Omega_S}. \quad (14c)$$

- **Approximation property:** if the solution \tilde{u} above belongs to $H^{s+1}(\Omega_S)^2$, for some exponent $s \geq 1$, then there is a constant C independent of ν and the mesh size h such that for any $v \in V_h$

$$|a_{S,h}(\tilde{u} - \Pi_h \tilde{u}, v)| \leq C \nu h^{\min(s,k)} \|\tilde{u}\|_{H^{s+1}(\Omega_S)} \|v\|_{1,h}. \quad (14d)$$

We combine the DG bilinear form for Stokes domain with the interface and Darcy forms to obtain the discrete bilinear form

$$a_h(u, v) = a_D(u, v) + a_I(u, v) + a_{S,h}(u, v). \quad (15)$$

With this form, we associate the energy norm

$$\|u\| = \left(\nu \|u\|_{1,h}^2 + \|K^{-1/2}u\|_{\Omega_D}^2 + \|\gamma^{1/2}K^{-1/4}u\|_{\Gamma_{SD}}^2 \right)^{1/2}. \tag{16}$$

Formally, the scheme is: find $(u_h, p_h) \in V_h \times Q_h$ such that

$$\begin{aligned} a_h(u_h, v) + b(v, p_h) &= (f_S, v)_{\Omega_S} \quad \forall v \in V_h, \\ b(u_h, q) &= (f_D, q)_{\Omega_D} \quad \forall q \in Q_h. \end{aligned} \tag{17}$$

By choosing the spaces V_h and Q_h such that Assumption 1 holds, the second line of this equation implies, that if $f_D = 0$, then also $\nabla \cdot u_h \equiv 0$ inside all grid cells, and thus $\nabla \cdot u_h = 0$ strongly.

3.2. Concrete methods

The projection operator in Assumption 2 is commonly known as the Fortin projection (see e.g. [9,16]) for divergence-conforming finite element spaces. Examples for such spaces are RT [26], BDM [8], BDFM [7] and the more recent ABF [3] spaces. They all consist of special polynomial spaces on each mesh cell, together with node functionals and transformations ensuring global H^{div} -conformity of the space. The matching pressure spaces are discontinuous piecewise polynomial functions (see Table 1). While the estimates in L^2 (9a) and H^{div} (9b) are classical, the broken H^1 -estimate (10) can be found in [12,13,17,18].

Discontinuous Galerkin schemes satisfying assumptions are the primal DG methods and the LDG methods [4]. For example, we define below the bilinear form $a_{S,h}$ used in the interior penalty method [2,28] and its variations, which is the method used in the numerical experiments in Section 5. Further notation is introduced. The pointwise average of a discontinuous function across interfaces is denoted by $\{\{ \cdot \}\}$ and for each face $F \in \Gamma_h^S$, a unit normal vector is chosen and denoted formally by n_h below

$$a_{S,h}(u, v) = 2\nu(D(u), D(v))_{\Gamma_h^S} - 2\nu\langle \{\{D(u)\}\} n_h, \llbracket v \rrbracket \rangle_{\Gamma_h^S} - 2\nu\langle \{\{D(v)\}\} n_h, \llbracket u \rrbracket \rangle_{\Gamma_h^S} + \frac{\sigma k^2}{h} \langle \llbracket u \rrbracket, \llbracket v \rrbracket \rangle_{\Gamma_h^S} + \frac{2\sigma k^2}{h} \langle u, v \rangle_{\Gamma_S}$$

The form $a_{S,h}$ satisfies Assumption 3.

In the next section, we analyze the scheme (17).

4. Analysis of the method

We first establish well-posedness of the scheme by proving an inf-sup condition. Then, we derive error estimates in the energy norm.

Lemma 1. *There is a constant $\beta > 0$ independent of h such that*

$$\inf_{q_h \in Q_h} \sup_{v_h \in V_h} \frac{b(v_h, q_h)}{\|v_h\| \|q_h\|_{\Omega}} \geq \beta^{-1}. \tag{18}$$

Proof. Fixing $q_h \in Q_h$ and it is sufficient to show that there is $v_h \in V_h$ such that

$$b(v_h, q_h) = \|q_h\|_{\Omega}^2 \quad \text{and} \quad \|v_h\| \leq \beta \|q_h\|_{\Omega}. \tag{19}$$

By the continuous inf-sup condition on the spaces $(H^1(\Omega), L_0^2(\Omega))$, there is a function $v \in (H^1(\Omega))^d$ such that

$$\nabla \cdot v = -q_h, \quad \text{in } \Omega, \tag{20}$$

$$v = 0, \quad \text{on } \partial\Omega, \tag{21}$$

and there is a positive constant C_0 such that

$$\|\nabla v\|_{\Omega} \leq C_0 \|q_h\|_{\Omega}. \tag{22}$$

Then, we have

$$b(v, q_h) = - \int_{\Omega} q_h \nabla \cdot v = \|q_h\|_{\Omega}^2.$$

Let $\Pi_h v$ be the interpolant in Assumption 2. Since $P_h q_h = q_h$, we obtain from (8):

$$b(\Pi_h v, q_h) = b(v, q_h) = \|q_h\|_{\Omega}^2,$$

and due to Poincaré’s inequality, as well as (9c) and (22), there are positive constants C_1, C_2, C_3 such that

$$\|\Pi_h v\|_{\Omega_D} \leq C_1 \|q_h\|_{\Omega},$$

$$\|\Pi_h v\|_{\Gamma_{SD}} \leq C_2 \|q_h\|_{\Omega},$$

$$\|\Pi_h v\|_{1,h} \leq C_3 \|q_h\|_{\Omega}.$$

Thus, we conclude that (19) holds with $v_h = \Pi_h v$ and

$$\beta = C_0 \left(\nu C_3^2 + K^{-1} C_1^2 + \gamma K^{-1/2} C_2^2 \right)^{1/2}. \quad \square \quad (23)$$

The inf-sup condition (18) and the coercivity assumption (14b) imply by standard arguments (see e.g. [9]) the following lemma.

Lemma 2. *There exists a unique solution $(u_h, p_h) \in V_h \times Q_h$ satisfying (17).*

Lemma 3. *Let (u, p) and (u_h, p_h) be the solutions to (5) and (17), respectively. Assume that $u \in H^{s+1}(\Omega)$ and $p \in H^{s+1}(\Omega)$ for some $s \geq 1$. Then, there is a constant C independent of the mesh size, ν and K , such that*

$$\| \|u_h - \Pi_h u\| \| \leq C \max(K^{-1}, K^{-1/2}) (1 + \nu^{1/2}) h^{\min(k,s)} \|u\|_{H^{s+1}(\Omega)}. \quad (24)$$

Proof. Define

$$\eta = u_h - \Pi_h u, \quad \xi = u - \Pi_h u, \quad (25)$$

$$\zeta = p_h - P_h p, \quad \chi = p - P_h p. \quad (26)$$

The error equation is: for all $v \in V_h$ and $q \in Q_h$:

$$a_h(\eta, v) + b(v, \zeta) = a_h(\xi, v) + b(v, \chi), \quad (27)$$

$$b(\eta, q) = b(\xi, q). \quad (28)$$

Choose $v = \eta$ and $q = \zeta$ and use coercivity (14b) of $a_{S,h}$:

$$\min(1, \alpha) \| \eta \| ^2 \leq a_h(\xi, \eta) + b(\eta, \chi) - b(\xi, \zeta).$$

From (7), we have $b(\eta, \chi) = 0$ and from (8), we have $b(\xi, \zeta) = 0$. From (14d), we have the bound:

$$a_{S,h}(\xi, \eta) \leq C \nu h^{\min(s,k)} \|u\|_{H^{s+1}(\Omega_s)} \| \eta \|_{1,h} \leq \frac{1}{2} \min(1, \alpha) \nu \| \eta \|_{1,h}^2 + C \nu h^{2\min(s,k)} \|u\|_{H^{s+1}(\Omega_s)}^2$$

The remaining terms are bounded as:

$$a_D(\xi, \eta) + a_I(\xi, \eta) \leq \frac{1}{2} \min(1, \alpha) (\|K^{-1/2} \eta\|_{\Omega_D}^2 + \gamma K^{-1/2} \| \eta \|_{\Gamma_{SD}}^2) + C (\| \xi \|_{\Omega_D}^2 + \| \xi \|_{\Gamma_{SD}}^2).$$

We then conclude by combining the bounds above and by using the approximation properties (11a) and (11b). \square

Theorem 1. Under the assumptions of Lemma 3 and $p \in H^{s+1}(\Omega)$, we obtain for C independent of h, ν, K :

$$\| \|u_h - u\| \| \leq C h^{\min(k,s)}, \quad \vartheta(\nu, K) \|u\|_{H^{s+1}(\Omega)},$$

$$\| \nabla \cdot u - \nabla \cdot u_h \| \leq C h^{\min(k+1,s)}, \quad \|u\|_{H^{s+1}(\Omega)},$$

$$\| p - p_h \| \leq C h^{\min(k,s)} \left(\beta \vartheta(\nu, K) \|u\|_{H^{s+1}(\Omega)} + \|p\|_{H^{s+1}(\Omega)} \right),$$

where β is the inf-sup constant from Lemma 1 and

$$\vartheta(\nu, K) = (1 + \nu^{1/2}) (1 + \max(K^{-1}, K^{-1/2})).$$

Proof. The first bound is obtained by a triangle inequality and (11c) in Assumption 2. The second bound is a consequence of (7) and approximation properties: for any $v \in V_h$, we have $\nabla \cdot v \in Q_h$ and therefore,

$$\| \nabla \cdot u - \nabla \cdot u_h \| ^2 = (\nabla \cdot u - \nabla \cdot u_h, \nabla \cdot u - \nabla \cdot v)_\Omega \leq \| \nabla \cdot u - \nabla \cdot u_h \| \| \nabla \cdot u - \nabla \cdot v \|.$$

Thus

$$\| \nabla \cdot u - \nabla \cdot u_h \|_{L^2(\Omega)} \leq \min_{v \in V_h} \| \nabla \cdot u - \nabla \cdot v \|_{L^2(\Omega)}.$$

Finally, the error estimate for the pressure is a consequence of the inf-sup condition in Lemma 1. \square

5. Numerical results

The numerical results below are computed with the interior penalty method on meshes consisting of squares for simplicity. In that case, the stability limit for σ is computable and we take twice this value, namely $\sigma = (k+1)(k+2)/h$, where h is

the length of the cell perpendicular to the edge. We use the viscosity $\nu = 1$ and $\gamma = 0.1$ in the Beavers–Joseph–Saffman condition, following [6].

First, we choose a problem with a smooth solution to show that the convergence rates are optimal with respect to mesh size. To this end, consider a geometry resembling flow through a porous filter as in Fig. 1. We choose no-slip (normal and tangential velocities prescribed) boundary conditions with a quartic inflow and outflow profile on the left and right boundaries of the domain, such that u_x and $\partial_y u_x$ vanish at the upper and lower boundaries. Thus, we are consistent with the slip (only normal velocities fixed) boundary condition on the top and bottom and the solution exhibits only mild singularities in the corners. Note that the slip boundary condition is also the well-posed condition on the normal velocity in the porous medium. Since all flow has to go through the filter in the center, the flow speed there is asymptotically independent of K as K tends to zero.

Results for the pair $\mathbb{RT}_1/\mathbb{Q}_1$ -element and permeability $K = 10^{-4}$ are reported in Table 2. Since the exact solution is unknown, we present the L^2 -norm of intrinsic errors obtained by taking the difference d_ℓ between numerical solutions on consecutive grid levels $\ell - 1$ and ℓ . Here, level 1 consists of 3×3 squares and higher levels are obtained by refining the squares of the previous levels into four congruent children.

The intrinsic convergence rates are obtained from these by the formula $r_\ell = \log_2(d_{\ell-1}/d_\ell)$. Note that in case of geometric error reduction (constant convergence rates), the intrinsic error is equivalent to the standard error and only differs by a fac-

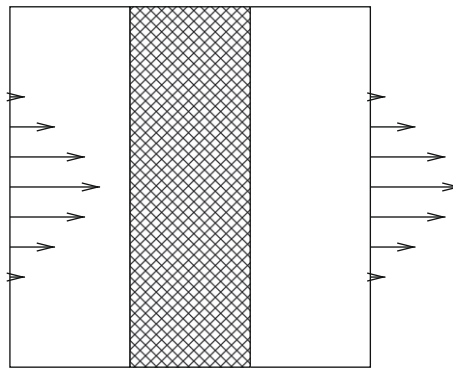


Fig. 1. Configuration for smooth solution. Free flow regions left and right separated by a porous medium. No-slip boundary conditions with quartic inflow and outflow profile left and right, slip at top and bottom.

Table 2

Intrinsic mean quadratic errors and convergence rates for the smooth problem solved with the $\mathbb{RT}_1/\mathbb{Q}_1$ -element pair ($\nu = 1, K = 10^{-4}$).

level	u_S		u_D		p_S		p_D		$\nabla \cdot u$
	Error	Rate	Error	Rate	Error	Rate	Error	Rate	
2	1.97e-01	–	1.45e-03	–	5.80e+00	–	2.23e+00	–	5.92e-12
3	4.60e-02	2.10	8.29e-05	4.13	3.65e-01	3.99	1.30e-01	4.10	1.79e-12
4	1.30e-02	1.83	1.82e-05	2.19	8.22e-02	2.15	2.91e-02	2.16	8.11e-13
5	3.43e-03	1.92	4.52e-06	2.01	2.05e-02	2.00	7.25e-03	2.00	4.68e-13
6	8.90e-04	1.95	1.14e-06	1.98	5.19e-03	1.98	1.83e-03	1.98	2.17e-13
7	2.27e-04	1.97	2.88e-07	1.99	1.31e-03	1.99	4.62e-04	1.99	1.34e-13

Table 3

Intrinsic convergence rates for higher order elements ($\nu = 1, K = 10^{-4}$).

Degree	Level	u_S	u_D	p_S	p_D
\mathbb{RT}_2	3	1.61	3.13	1.92	2.99
	4	2.82	3.26	2.29	3.04
	5	2.97	3.12	2.38	3.03
	6	3.00	3.04	2.42	3.01
\mathbb{RT}_3	3	3.73	4.36	3.60	4.36
	4	3.80	3.91	3.24	4.00
	5	3.85	4.13	3.10	3.99
	6	3.88	4.33	3.04	4.00
\mathbb{RT}_4	3	4.05	5.50	3.03	5.32
	4	4.03	5.07	3.00	4.98

tor. The table shows, that in spite of the fact that the energy norm involves the derivatives of u_S and the field u_D itself, the mean quadratic errors of both converge with the optimal order 2. The same is true for the pressure in both subdomains. Thus, we conclude that the scheme is well balanced and convergence in the subdomains is not impeded by the coupling.

The boundary conditions in this particular example were chosen such that the solutions for velocity and pressure are smooth. In Table 3, we show intrinsic convergence rates for higher order elements. The observed rates for the velocities are $k + 1$ as predicted; the reduced orders for u_S with \mathbb{RT}_4 are due to lack of regularity of the solution (see Fig. 2). The pressure p_D exhibits order $k + 1$, as predicted by the theory for the Raviart–Thomas element for the mixed Laplacian. The convergence rate for the pressure p_S confirms our analysis. We note that trivially the order of convergence of the global pressure corresponds to our error estimates.

Next, we study the robustness of the errors with respect to the permeability K . Fig. 3 clearly shows robustness of the relative error of the Stokes solution with respect to permeability. The relative error of the Darcy solution decays linearly with

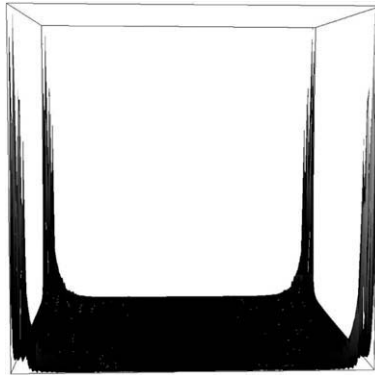


Fig. 2. Intrinsic velocity error distribution for $\mathbb{RT}_4/\mathbb{Q}_4$, exhibiting the weak corner singularities.

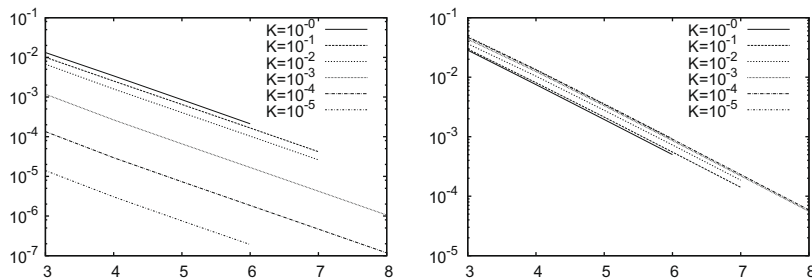


Fig. 3. Relative errors of u_D (left) and u_S (right) depending on refinement level for different permeabilities K .

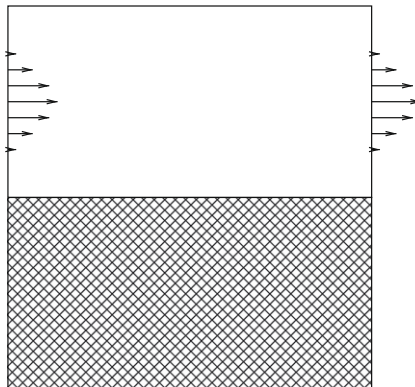


Fig. 4. Setup for flow in a river bed. The Stokes region is on top and the Darcy region on the bottom. Slip conditions left, right and bottom, no-slip at the top.

permeability. This is caused by the fact that the norm of u_D is nearly independent of K (all flow has to go through the filter), but the error scales with K^{-1} .

In a second test, we consider an idealized flow in a river bed as depicted in Fig. 4. The free-flow subdomain is on top, the porous medium at the bottom. On the top boundary, we fix normal and tangential velocities (no-slip), on the others only the tangential velocity. The quartic inflow and outflow profiles in the Stokes region are chosen such that no singularity is triggered at the interface ($u = \partial_n u = 0$). This example differs from the previous in that the flow speed in the porous medium depends strongly on the permeability; for small permeabilities linearly. Since the flow is driven by the flow in the Stokes subdomain, where errors are expected to be independent of permeability, we expect the absolute errors of the Darcy velocity to reduce if K tends to zero. Nevertheless, since the solution there diminishes as well, this prediction might be wrong for the relative error. Indeed, in our experiment the absolute error on fine meshes behaves like $K^{1/2}$, such that the relative error grows with $K^{-1/2}$. This is confirmed by Fig. 5.

Finally, we confirm that the method is strongly conservative, even in the case of non-tangential flow across the interface. To this end, consider the configuration in Fig. 6. The left half of the domain is the free-flow part with Stokes equations, a

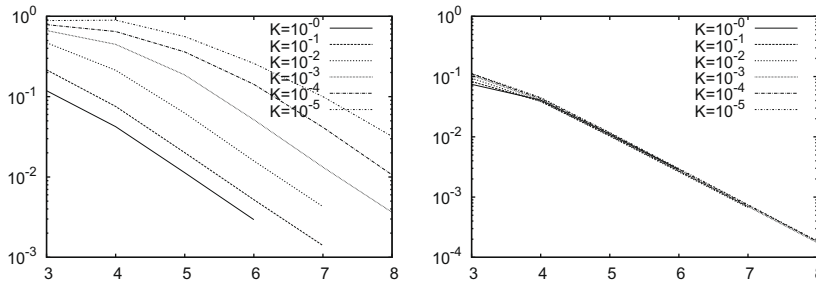


Fig. 5. Relative errors of u_D (left) and u_S (right) in the river bed example depending on refinement level for different permeabilities K .

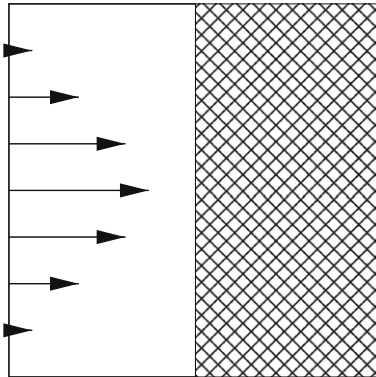


Fig. 6. Configuration for mass conservation test. The thick boundary on the left half of the domain indicates no-slip, the dashed boundary on the right prescribed pressure $p = 0$.

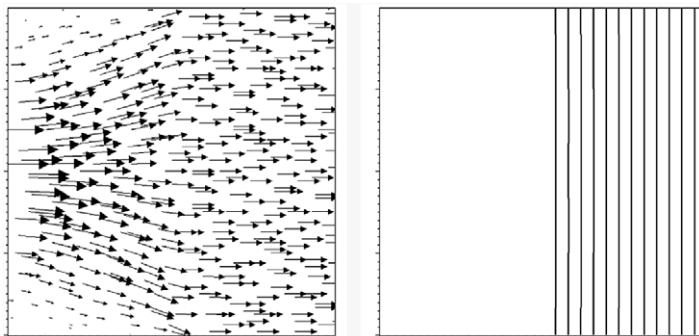


Fig. 7. Velocity field and pressure isolines for the mass conservation test with $K = 10^{-4}$.

Table 4

Mass flux difference between inflow and outflow side of the domain.

Level	$K = 10^{-2}$	$K = 10^{-4}$	$K = 10^{-6}$
2	1.4e-08	8.5e-10	1.2e-09
3	2.5e-10	2.7e-10	5.1e-11
4	4.5e-10	1.2e-09	4.7e-09

quadratic inflow profile and no-slip boundary conditions. The Darcy part on the right has slip conditions on the top and bottom and pressure boundary condition $p = 0$ on the right. Accordingly, the normal flux $u \cdot n$ on the right boundary is a result of the computation. The velocity and pressure solution for this problem are shown in Fig. 7. It is important to note that such non-tangential flow across the interface was not experimentally considered in [6]. Tangential flow is sufficient (but not necessary) for the Beavers–Joseph–Saffman law to hold. For non-tangential flows, in particular in filtration problems [25], the law is still accepted even though there is no experimental evidence that confirms or denies the use of this law. A mathematical justification of the Beavers–Joseph–Saffman law for non-tangential flow can be obtained by applying homogenization techniques found in [20,21] according to Mikelič but this will be very technical.

Since the strong, homogeneous, normal boundary conditions on top and bottom assure that no mass is lost there, we use the difference of the integrals of the normal flux over the left and right boundaries, respectively, to demonstrate the conservation property of our method. With an incoming flux integral of $4/3$, the results displayed in Table 4 show clearly that the mass flux error is close to the computational accuracy and thus confirms the strong conservation property of the method.

6. Conclusions

We presented a uniform finite element method for the coupling of Stokes and Darcy flow. By the use of divergence-conforming elements, exact mass conservation is guaranteed. We presented an error norm estimate which is optimal with respect to the approximation spaces, but suggests an imbalance between the subdomains. The results of the numerical experiments on the other hand indicate, that the scheme is indeed well balanced and convergence orders in L^2 are the same for the Stokes and the Darcy part. The proof of this convergence requires more involved analysis and will be postponed to a future article.

Acknowledgments

The numerical results in this article were produced using the deal.II finite element library [5]. The authors would like to thank Willi Jäger and Andro Mikelič for sharing their insight in coupling conditions.

References

- [1] T. Arbogast, D. Brunson, A computational method for approximating a Darcy–Stokes system governing a vuggy porous medium, *Comput. Geosci.* 11 (2007) 207–218.
- [2] D.N. Arnold, An interior penalty finite element method with discontinuous elements, *SIAM J. Numer. Anal.* 19 (4) (1982) 742–760.
- [3] D.N. Arnold, D. Boffi, R.S. Falk, Approximation by quadrilateral finite elements, *Math. Comput.* 71 (2002) 909–922.
- [4] D.N. Arnold, F. Brezzi, B. Cockburn, D. Marini, Unified analysis of discontinuous Galerkin methods for elliptic problems, *SIAM J. Numer. Anal.* 39 (5) (2001) 1749–1779.
- [5] W. Bangerth, R. Hartmann, G. Kanschat, Deal. II—a general purpose object oriented finite element library, *ACM Trans. Math. Softw.* 33 (4) (2007).
- [6] G.S. Beavers, D.D. Joseph, Boundary conditions at a naturally impermeable wall, *J. Fluid. Mech.* 30 (1967) 197–207.
- [7] F. Brezzi, J. Douglas, M. Fortin, D. Marini, Efficient mixed finite element methods in two and three space variables. *RAIRO Modél. Math. Anal. Numer.* 21 (1987) 581–604.
- [8] F. Brezzi, J. Douglas, D. Marini, Two families of mixed finite elements for second order elliptic problems, *Numer. Math.* 47 (1985) 217–235.
- [9] F. Brezzi, M. Fortin, *Mixed and Hybrid Finite Element Methods*, Springer, 1991.
- [10] E. Burman, P. Hansbo, Stabilized Crouzeix–Raviart elements for the Darcy–Stokes problem, *Numer. Methods Partial Diff. Eqn.* 21 (2005) 986–997.
- [11] E. Burman, P. Hansbo, A unified stabilized method for Stokes and Darcy’s equations, *J. Comput. Appl. Math.* 198 (1) (2007) 35–51.
- [12] B. Cockburn, G. Kanschat, D. Schötzau, A locally conservative LDG method for the incompressible Navier–Stokes equations, *Math. Comput.* 74 (2005) 1067–1095.
- [13] B. Cockburn, G. Kanschat, D. Schötzau, A note on discontinuous Galerkin divergence-free solutions of the Navier–Stokes equations, *J. Sci. Comput.* 31 (1–2) (2007) 61–73.
- [14] M. Discacciati, E. Migliorini, A. Quarteroni, Mathematical and numerical models for coupling surface and groundwater flows, 19th Dundee Biennial Conference on Numerical Analysis, *Appl. Numer. Math.* 43 (1–2) (2001) 57–74.
- [15] G. Gatica, S. Meddahi, R. Oyarzua, A conforming mixed finite-element method for the coupling of fluid flow with porous media flow, *IMA J. Numer. Anal.* 29 (2009) 86–108.
- [16] V. Girault, P.-A. Raviart, *Finite Element Approximations of the Navier–Stokes Equations*, Springer, 1986.
- [17] V. Girault, B. Rivière, DG approximation of coupled Navier–Stokes and Darcy equations by Beaver–Joseph–Saffman interface condition, *SIAM J. Numer. Anal.* (2007).
- [18] P. Hansbo, M.G. Larson, Discontinuous Galerkin methods for incompressible and nearly incompressible elasticity by Nitsche’s method, *Comput. Methods Appl. Mech. Eng.* 191 (2002) 1895–1908.
- [19] N. Hanspal, A. Waghode, V. Nassehi, R. Wakeman, Numerical analysis of coupled Stokes/Darcy flows in industrial filtrations, *Transport Porous Med.* 64 (1) (2006) 1573–1634.
- [20] W. Jäger, A. Mikelič, On the boundary conditions at the contact interface between a porous medium and a free fluid, *Ann. Scuola Norm. Sup. Pisa Cl. Sci.* (4) 23 (3) (1996) 403–465.

- [21] W. Jäger, A. Mikelić, On the interface boundary condition of Beavers, Joseph, and Saffman, *SIAM J. Appl. Math.* 60 (4) (2000) 1111–1127 (electronic).
- [22] W. Jäger, A. Mikelić, Modeling effective interface laws for transport phenomena between an unconfined fluid and a porous medium using homogenization, *Transp. Porous Med.* 78 (3) (2009) 489–508. <http://dx.doi.org/10.1007/s11242-009-9354-9>.
- [23] G. Kanschat, *Discontinuous Galerkin Methods for Viscous Flow*, Deutscher Universitätsverlag, Wiesbaden, 2007.
- [24] W.J. Layton, F. Schieweck, I. Yotov, Coupling fluid flow with porous media flow, *SIAM J. Numer. Anal.* 40 (6) (2003) 2195–2218.
- [25] V. Nassehi, Modelling of combined Navier–Stokes and Darcy flows in crossflow membrane filtration, *Chem. Eng. Sci.* 53 (6) (1998) 1253–1265.
- [26] P.-A. Raviart, J.M. Thomas, A mixed method for second order elliptic problems, in: I. Galligani, E. Magenes (Eds.), *Mathematical Aspects of the Finite Element Method*, Springer, New York, 1977, pp. 292–315.
- [27] B. Rivière, Analysis of a discontinuous finite element method for the coupled Stokes and Darcy problems, *J. Sci. Comput.* 22 (2005) 479–500.
- [28] B. Rivière, M.F. Wheeler, V. Girault, A priori error estimates for finite element methods based on discontinuous approximation spaces for elliptic problems, *SIAM J. Numer. Anal.* 39 (3) (2001) 902–931.
- [29] B. Rivière, I. Yotov, Locally conservative coupling of Stokes and Darcy flow, *SIAM J. Numer. Anal.* 42 (2005) 1959–1977.
- [30] P. Saffman, On the boundary condition at the surface of a porous media, *Stud. Appl. Math.* 50 (1971) 292–315.
- [31] J. Wang, X. Ye, New finite element methods in computational fluid dynamics by $H(\text{div})$ elements, *SIAM J. Numer. Anal.* 45 (2007) 1269–1286.